

RECONSTRUCTING EVOLVING SIGNALLING NETWORKS BY HIDDEN MARKOV NESTED EFFECTS MODELS¹

BY XIN WANG, KE YUAN, CHRISTOPH HELLMAYR, WEI LIU
AND FLORIAN MARKOWETZ

University of Cambridge

Inferring time-varying networks is important to understand the development and evolution of interactions over time. However, the vast majority of currently used models assume direct measurements of node states, which are often difficult to obtain, especially in fields like cell biology, where perturbation experiments often only provide indirect information of network structure. Here we propose hidden Markov nested effects models (HM-NEMs) to model the evolving network by a Markov chain on a state space of signalling networks, which are derived from nested effects models (NEMs) of indirect perturbation data. To infer the hidden network evolution and unknown parameter, a Gibbs sampler is developed, in which sampling network structure is facilitated by a novel structural Metropolis–Hastings algorithm. We demonstrate the potential of HM-NEMs by simulations on synthetic time-series perturbation data. We also show the applicability of HM-NEMs in two real biological case studies, in one capturing dynamic crosstalk during the progression of neutrophil polarisation, and in the other inferring an evolving network underlying early differentiation of mouse embryonic stem cells.

1. Introduction. Understanding the inner workings of a complex system in biology, ecology and many other fields often relies on interventions to the system as well as subsequent observation and analysis of perturbation effects. For example, in biology, gene silencing such as RNA interference (RNAi) followed by phenotypic screening has become a widely used approach to study functions of genes and the signalling interactions between them [Boutros and Ahringer (2008)]. Recently, there is an increasing interest in generating and analysing time-series phenotypic screens after perturbations of a signalling network in order to study dynamics of a biological system over time [Ivanova et al. (2006), Neumann et al. (2010), Ku et al. (2012)]. Despite some success in time-series analysis as well as graphical modelling, there is still a lack of methodology specifically targeting this type of data to reconstruct time-varying signalling networks.

Received March 2013; revised September 2013.

¹Supported in part by The University of Cambridge, Cancer Research UK and Hutchison Whampoa Limited.

Key words and phrases. Dynamic, signalling networks, gene perturbation, hidden Markov, nested effects models, MCMC.

1.1. *Related work.* Recently, a lot of effort has been put into extending graphical models to infer evolving networks. In 2006, a generalised exponential random graph model (ERGM) was proposed to model the temporal progression of social networks [Hanneke and Xing (2006)]. ERGM was further extended to a hidden temporal ERGM (htERGM) by considering the networks as latent variables and using a local kernel-weighting technique to learn smoothly evolving graphical Gaussian models [Guo et al. (2007)]. It was also proposed to model discrete time-varying graphs as evolving Markov random fields and perform graphical regression under smoothness assumption with l_1 shrinkage [Ahmed and Xing (2009)]. Another major group of models in this field are dynamic Bayesian networks (DBNs). The original DBN was developed under the assumption of a homogeneous Markov chain [Murphy (2002)]. Nonstationary continuous DBNs were developed recently by assuming a fixed network with varying interaction parameters [Grzegorzcyk and Husmeier (2009)]. Network structures are allowed to change in nonstationary DBNs for discrete data [Robinson and Hartemink (2009)]. Nonhomogeneous DBNs were proposed to consider evolving networks as multiple changepoint regression models and use reversible jump MCMC methods to do inference [Lèbre (2007)]. Further improvements of nonhomogeneous DBNs were made by introducing information sharing among time series segments [Husmeier, Dondelinger and Lebre (2010)]. Moreover, a time-varying DBN (TV-DBN) model was proposed to infer directed time-varying network structure by a kernel-weighting l_1 -regularised auto-regressive approach [Song, Kolar and Xing (2009)].

These models have their own advantages and were all demonstrated to be effective in specific applications. Their common limitation, however, is that they reconstruct time-varying networks from direct observations of nodes, which in cell biology are often difficult to obtain. For example, measuring activities of signalling proteins in a cellular pathway is very difficult, as they are mostly mediated by post-translational modifications, which are usually not visible in gene expression data, the most commonly used data for network inference [Markowetz (2010)].

Markowetz, Bloch and Spang (2005) addressed this problem by introducing nested effect models (NEMs) to reconstruct signalling networks from observations of downstream genes whose expression levels are affected by perturbations of signalling proteins. The name nested effect models stems from the fact that NEMs infer directed relations between signalling proteins by *subset relations* between their perturbation effects [Markowetz et al. (2007)]. Since their introduction [Markowetz, Bloch and Spang (2005), Markowetz et al. (2007)], static NEMs have been extended in different directions and have been applied in several case studies [Fröhlich et al. (2007, 2008), Tresch and Markowetz (2008), Vaske et al. (2009), Anchang et al. (2009), House et al. (2010), Fröhlich, Praveen and Tresch (2011), Niederberger et al. (2012), Sadeh, Moffa and Spang (2013), Failmezger et al. (2013)].

NEMs have been extended to model dynamics within signalling pathways under the assumption that the observed dynamic perturbation effects over time are due to time delay of signal transduction [Anchang et al. (2009)]. Another extension of NEMs infers time-varying networks by unrolling the network structure over time [Fröhlich, Praveen and Tresch (2011), Failmezger et al. (2013)].

1.2. Contributions of this article. We propose the hidden Markov nested effects models (HM-NEM) to infer time-varying signalling networks. The evolving network is modelled as a discrete time first-order Markov process. The state space corresponds to all possible network topologies. The transition probabilities of the Markov process are defined by a geometric distribution, which exploits the topological distance (defined as the distance between their adjacency matrices) between networks. Similar to the “smoothness” assumption in TV-DBNs, we assume that the more distant two networks are, the less likely the transition is. Importantly, such “smoothness” is controlled by a parameter which can be estimated from the data. For the observation model, NEMs provide the formulation of emission probabilities that link the hidden network topologies to the observable perturbation effects.

From a Bayesian perspective, the inference target is the joint posterior distribution of the time-varying networks and the unknown smoothness parameter, given the observed effects. To approach the target distribution, we propose a Gibbs sampler based on “Metropolis-within-Gibbs”. The algorithm alternates between sampling the state path and the parameter from the corresponding full conditionals.

In the next section, we briefly describe nested effects models and introduce the marginal likelihood as well as inference methods. The description and inference method of HM-NEM are presented in Sections 2.2 and 3, respectively. In Section 4 we demonstrate simulation studies including convergence diagnosis, sensitivity and coverage analysis on synthetic data for networks with slow, moderate and rapid transitions. Finally, we show two applications of HM-NEM to reconstruct the polarisation network of neutrophils in Section 5.1 and the self-renewal signalling network of embryonic stem cells in Section 5.2.

2. Model.

2.1. Background. Nested effects models (NEMs) are a statistical approach that is specifically tailored to reconstruct features of pathways from perturbation effects in downstream reporters [Markowitz et al. (2007)]. In contrast to other graphical models, which are all based on measures of pairwise association (e.g., coexpression networks) and encode conditional independence relations (e.g., Bayesian networks), NEMs describe *subset relationships* between observed downstream effects of perturbations.

To describe NEMs more clearly, we show a toy signalling network [Figure 1(A)] consisting of a kinase (A) and three transcription factors (B, C and D), which directly regulate reporter genes (1 to 10). Phenotypic data generally do not include

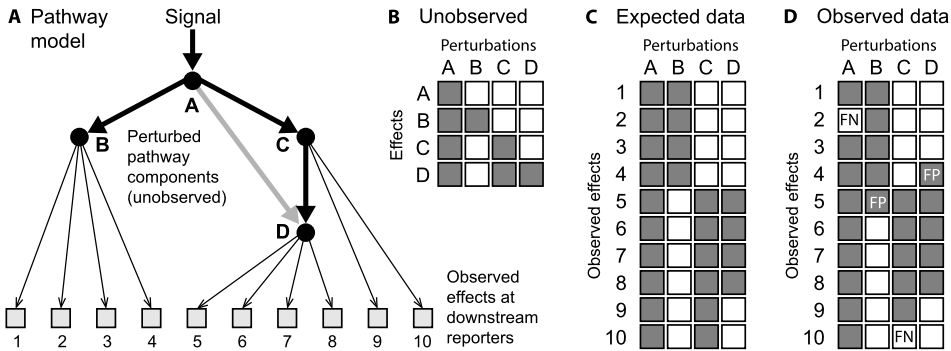


FIG. 1. A schematic figure of nested effects models. (A) A toy example of NEMs. Perturbed pathway components (often called S-genes, referring to the signalling genes that are silenced by perturbations) and effect reporters (called E-genes if they are transcriptional) are shown in black round circles and grey rectangles, respectively. The thick black arrows between pathway components denote their signalling relationships, while the thin black arrows connect pathway components to their direct effect reporters. The thick grey arrow between pathway components A and D is a transitive edge indicating an indirect effect of A on D (via C). (B) States of pathway components upon different perturbations are generally unobserved. A pathway component is in the state of 0 (white rectangle) if it is not perturbed, and in the state of 1 (black rectangle) if it is perturbed directly or by a perturbation propagated down from an upstream component. (C) The expected states of effect reporters (black = effect; white = no effect) after perturbing pathway components. (D) In real biological applications, the noisy measurement of effect reporter states may include false negatives (FNs) and false positives (FPs).

the states of proteins A to D after perturbations [Figure 1(B)]. This is because phenotypes like gene expression or cell morphologies are downstream of the pathway of interest and often do not contain much information on the activity states of the proteins in the pathway.

NEMs assume that perturbing upstream pathway components may impact a global process, while silencing downstream genes only affect local subprocesses. This results in a subset pattern in the observed data. For example, for the pathway in Figure 1(A) the perturbation effects (e.g., expression changes in reporter genes) of pathway components B, C and D are subsets of the effect of gene A: perturbing A has an effect on all reporters (1–10), while perturbing B only affects reporters 1–4, perturbing C affects reporters 5–10, and perturbing D affects reporters 5–8 [Figure 1(C)].

NEMs leverage the observed data on effect reporters [Figure 1(D)] and infer the most likely pathway structure that can explain the subset patterns by comparing it to the data expected for a pathway [Figure 1(C)]. If the data are transcriptional phenotypes of RNAi experiments (like in our second case study), the pathway components and effect reporters are also called S-genes and E-genes [Markowitz, Bloch and Spang (2005)].

A pathway component j is in the natural state of 0 ($S_{jk} = 0$) if it is not affected by perturbation k , and is in the state of 1 ($S_{jk} = 1$) if it is interrupted directly

by biological perturbation or indirectly by propagation of a perturbation from an upstream pathway component [e.g., Figure 1(B)]. In real biological applications, the perturbation can be either enhancing (e.g., by drug treatment in our application to neutrophil polarisation) or inhibiting (e.g., by RNAi in our application to mouse embryonic stem cell differentiation). Since data sets generally contain either one or the other of these perturbations, we do not distinguish between enhancing and inhibiting perturbations in the description of our method.

A signalling network is modelled by $G = (\mathcal{V}, \mathcal{E})$, in which \mathcal{V} is the set of pathway components and \mathcal{E} a set of all interactions between them. Let $D = [d_{ik}]_{m \times l}$ be the observed perturbation effects [e.g., Figure 1(D)], where d_{ik} is the effect of perturbation k on effect reporter i .

Transitivity. An important feature of NEMs is the transitivity of subset relations [Markowitz et al. (2007)]. For example, the perturbation effect of gene D is a subset of the effect of gene C, which is a subset of the effect of gene A [Figure 1(C)]. Then the perturbation effect of gene D must also be a subset of gene A. Thus, the graph encoding such transitive subset relations should be transitively closed: whenever there is a path from one pathway component to another one (e.g., $A \rightarrow C \rightarrow D$), a directed edge (e.g., $A \rightarrow D$) exists between these two pathway components in the graph.

Marginal likelihood. Here, we make a convenience assumption that each effect reporter is specific for only a single pathway component. Let $\Theta := \{\theta_i\}_1^m$, where $\theta_i \in \{1, \dots, n\}$, be a set of parameters indicating the positions of effect reporters. Reporter i is specific for component j if $\theta_i = j$. Usually, reporter positions are unknown; thus, the likelihood of the signalling network G given the observation D is computed by marginalisation over Θ :

$$\begin{aligned}
 P(D|G) &= \int P(D|G, \Theta) P(\Theta|G) d\Theta \\
 (2.1) \qquad &= \frac{1}{n^m} \prod_{i=1}^m \sum_{j=1}^n \prod_{k=1}^l P(d_{ik}|G, \theta_i = j),
 \end{aligned}$$

where the first product is over all effect reporters under the assumption that reporters are independent of each other, while the second product is over all replicates under the assumption that replicates are independent of each other. During marginalisation, each effect reporter is “attached” to all pathway components; we thus implicitly take multiple regulators into account (but not complex interactions between them).

For a single effect reporter i under perturbation k , the probability to observe d_{ik} given G and its position $\theta_i = j$ can be computed by

$$\begin{aligned}
 (2.2) \qquad & \qquad \qquad d_{ik} = 1 \quad d_{ik} = 0 \\
 P(d_{ik}|G, \theta_i = j) &= \begin{cases} \alpha & 1 - \alpha & S_{jk} = 0, \\ 1 - \beta & \beta & S_{jk} = 1, \end{cases}
 \end{aligned}$$

where α and β are global false positive and false negative rate of D that can often be estimated from control experiments [Markowitz, Bloch and Spang (2005)]; S_{jk} is the state of pathway component j upon perturbation k .

However, when the relationships between pathway components and effect reporters are already known, the likelihood can be simplified to

$$(2.3) \quad P(D|G) = \prod_{i=1}^m \prod_{k=1}^l P(d_{ik}|G).$$

Inference. The original NEM performs an exhaustive search over all transitively closed graphs to identify the optimal network by the maximum likelihood estimation [Markowitz, Bloch and Spang (2005)]. For large-scale networks consisting of many signalling genes, heuristics such as pairwise, triplets inference [Markowitz et al. (2007)] and module networks [Fröhlich et al. (2007, 2008)] have been developed. The definition of effects has also been extended, for example, by modelling differential expression as a mixture model of p -values [Fröhlich et al. (2007)] or log-ratios [Tresch and Markowitz (2008)]. Moreover, Niederberger et al. (2012) proposed an efficient inference method by combining MCMC sampling with an Expectation–Maximisation (EM) algorithm.

Maximum likelihood inference was adopted in the original NEM, while the model itself can be naturally extended by incorporating priors of the signalling network and/or the regulatory structure between signalling genes and reporter genes. Fröhlich et al. (2007) extended NEMs to take into account prior knowledge about network structure, and applied Bayesian regularisation using Akaike information criterion (AIC). Maximum *a posteriori* estimation was also proposed to incorporate prior network structure by Tresch and Markowitz (2008) and Fröhlich et al. (2008).

2.2. Hidden Markov nested effects model. As mentioned in Section 1, NEMs establish a framework for reconstruction of static signalling networks from perturbation effects. However, NEMs and their extensions do not allow network structure to change over time in their present forms. Here, we extend NEM to the Hidden Markov nested effects model (*HM-NEM*) to model signalling networks with topological changes over discrete time points.

The time-varying network is considered as a discrete stochastic process $G_{1:T} = \{G_t\}_1^T$. Let $G_t = (\mathcal{V}, \mathcal{E}_t)$ be the network at time t for $t \in \{1, \dots, T\}$, in which \mathcal{V} is the set of pathway components and \mathcal{E}_t is the edge set (throughout this paper edge means directed edge) including all signalling interactions between pathway components at timestep t . Let $D_{1:T} = \{D_t\}_1^T$, where $D_t = [d_{ikt}]_{m \times l}$ is a matrix of observed effects for m effect reporters across l perturbations. Under the first-order Markov assumption the probability of the observation of G_t only depends on its previous network structure G_{t-1} for $t \in \{2, \dots, T\}$ (the upper layer in Figure 2).

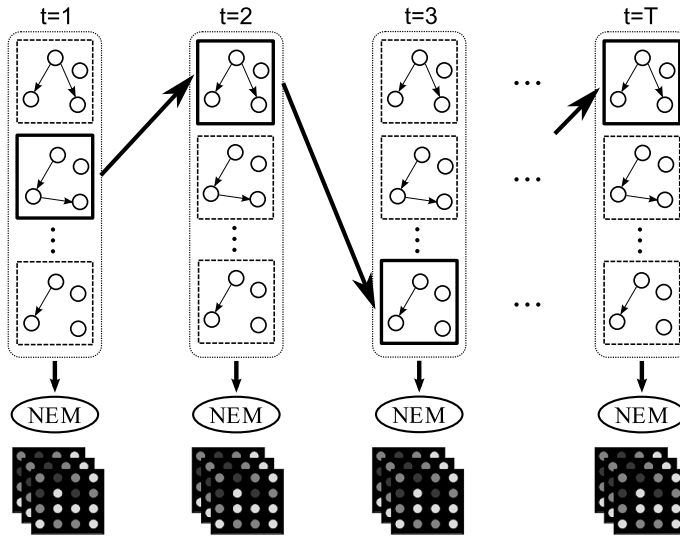


FIG. 2. A schematic figure describing the framework of HM-NEMs. HM-NEMs are comprised of a Markov chain modelling an evolving signalling network (the upper layer) and NEMs as the emission module (the middle layer). Images in the lower layer represent observed time-series perturbation effects. All possible networks for a given number of pathway components are included in the state space denoted by dotted rounded rectangles. At each time step, only one state is present and is highlighted by a thick black square. The state transitions between adjacent time points are highlighted by thick black arrows.

A hidden Markov nested effects model (HM-NEM) is a hidden Markov model (HMM) with the time-varying network as the transition module and nested effects model as the emission module. Similar to ordinary HMMs, we represent a HM-NEM as $\mathcal{H}_{\text{nem}} = (\pi, A, B)$, in which π is the initial distribution over states (network structures), and A and B denote the transition probabilities and emission probabilities, respectively. Since the state space of the hidden layer consists of *all* possible network structures, no model selection is needed to determine the number of states, which is fixed but can be very large (e.g., >1 billion states for a network consisting of only six pathway components).

Initial distribution. The initial distribution is set to be a uniform distribution over all the possible network structures. This setting makes the initial distribution take no part in the inference methods, reflecting the fact that prior information about the underlying network is often not available in gene perturbation studies.

Transition probability. We assume here that a signalling network prefers to transit to a state with a similar structure. That is, let P_{uv} be the probability to transit from state u to v , then the more distant the network structure v is from u , the lower the transition probability P_{uv} will be. This assumption is sound in biology, and many other graphical models for modelling time-varying networks also make

similar assumptions [e.g., TV-DBN in Song, Kolar and Xing (2009) and TESLA in Ahmed and Xing (2009)]. Here we use the geometric distribution to derive the transition probabilities:

$$(2.4) \quad P_{uv} = P(G_{t+1} = v | G_t = u) = \frac{1}{Z_u} (1 - \lambda)^{s_{uv}} \lambda,$$

where $Z_u = \sum_u (1 - \lambda)^{s_{uv}} \lambda$ is a normalising constant; $\lambda \in (0, 1)$ is a parameter controlling the “smoothness”; s_{uv} is the distance between network u and v computed by

$$(2.5) \quad s_{uv} = \|A^u - A^v\|_1 := \sum_r \sum_c |a_{rc}^u - a_{rc}^v|,$$

where A^u and A^v are binary adjacency matrices of networks u and v ; precisely, $a_{rc} = 1$ denotes a directed edge from vertice r to c , and 0 otherwise. Each G_t corresponds to a unique adjacency matrix A_t . In the following we show that this transition model is a special case of the htERGM in Guo et al. (2007).

Connection with the htERGM [Guo et al. (2007)]. The transition probability setting for the htERGM is

$$(2.6) \quad P(G_{t+1} | G_t) = \frac{1}{Z(\theta, G_t)} \exp\{\theta^T \Psi(G_{t+1}, G_t)\},$$

where $\Psi(G_t, G_{t-1})$ is a vector-valued function corresponding to several statistics of the two network topologies. The parameter θ contains the weights of these features.

To see that our transition model is a special case of the above, we rewrite equation (2.4) with the terminology of Guo et al. (2007):

$$\begin{aligned} P(G_t | G_{t-1}) &= \frac{1}{Z(\lambda, G_t)} \exp\left(\sum_r \sum_c |a_{rc}^{G_{t+1}} - a_{rc}^{G_t}| \ln(1 - \lambda) + \ln \lambda\right) \\ &= \frac{1}{Z(\lambda, G_t)} \exp\left([\ln \lambda, \ln(1 - \lambda)] \left[\sum_r \sum_c |a_{rc}^{G_{t+1}} - a_{rc}^{G_t}| \right]\right) \\ &= \frac{1}{Z(\theta, G_t)} \exp(\theta^T \Phi(G_{t+1}, G_t)), \end{aligned}$$

where

$$\theta = \begin{bmatrix} \ln \lambda \\ \ln(1 - \lambda) \end{bmatrix}, \quad \Psi = \left[\sum_r \sum_c |a_{rc}^{G_{t+1}} - a_{rc}^{G_t}| \right],$$

$$Z(\theta, G_t) = \sum_{G_{t+1}} \exp(\theta^T \Phi(G_{t+1}, G_t)).$$

Note that the second dimension of the feature vector Ψ directly tells the amount of changes between the two networks. Its corresponding weight parameter $\ln(1 - \lambda)$ can be used to generate/fit difference levels of network dynamics. This is consistent with our design for λ being the probability of an edge staying the same.

Emission probability. The emission probability in a HM-NEM is the probability to observe perturbation effects D_t at time t given the current network topology G_t , which can be derived directly from the marginal likelihood of the nested effects model in equation (2.1) when the relationships of pathway components to effect reporters are unknown:

$$(2.7) \quad P(D_t|G_t) = \frac{1}{n^m} \prod_{i=1}^m \sum_{j=1}^n \prod_{k=1}^l P(d_{ikt}|G_t, \theta_i = j).$$

Similarly, if the relationships between pathway components and effect reporters are already known, the emission probability can be derived from equation (2.3):

$$(2.8) \quad P(D_t|G_t) = \prod_{i=1}^m \prod_{k=1}^l P(d_{ikt}|G_t, \theta_i = j).$$

3. Inference. Having established the framework of HM-NEMs, our main interest is to infer the joint posterior distribution $P(G_{1:T}, \lambda|D_{1:T})$ of state sequence $G_{1:T}$ and the unknown parameter λ in equation (2.4) given the phenotype of gene perturbations over time $D_{1:T}$. To approach this target distribution, we use a Gibbs sampler which draws samples from the two full conditionals: $P(G_{1:T}|\lambda, D_{1:T})$ and $P(\lambda|G_{1:T}, D_{1:T})$.

Sampling $G_{1:T}$. The full conditional of states is obtained by a single-site-update approach, which samples one hidden state at a time. As such, letting $G_{-t} := \{G_{t'}; t' \neq t\}$, the target distribution becomes the conditional distribution of each state given all the other states, data and parameter, which can be written as

$$P(G_t = s|G_{-t}, D_{1:T}, \lambda) \propto \begin{cases} P(G_{t+1}|G_t = s, \lambda)P(D_t|G_t = s), & \text{if } t = 1, \\ P(G_t = s|G_{t-1}, \lambda)P(G_{t+1}|G_t = s, \lambda)P(D_t|G_t = s), & \text{if } t = 2, \dots, T - 1, \\ P(G_t = s|G_{t-1}, \lambda)P(D_t|G_t = s), & \text{if } t = T. \end{cases}$$

Direct sampling from this distribution is infeasible. Hence, we resort to the Metropolis-within-Gibbs approach [Geyer (2011)] which facilitates sampling by the Metropolis–Hastings (MH) algorithm.

To sample networks, we propose a structural MH. By contrast to the method in Madigan, York and Allard (1995), this MH does not restrict the state space to

DAGs. In detail, we use a uniform jumping distribution to propose new graphs: a new graph s' is generated by adding or deleting an edge selected randomly with equal probabilities from all pairs of genes in the current graph s .

The acceptance ratio of a proposed graph s' to s can be calculated by

$$\begin{aligned}
 \alpha_{G_t} &= \frac{P(G_t = s' | G_{-t}, D_{1:T}, \lambda) P(s | s')}{P(G_t = s | G_{-t}, D_{1:T}, \lambda) P(s' | s)} \\
 (3.1) \quad &= \begin{cases} \frac{P(G_{t+1} | G_t = s', \lambda) P(D_t | G_t = s')}{P(G_{t+1} | G_t = s, \lambda) P(D_t | G_t = s)}, & \text{if } t = 1, \\ \frac{P(G_t = s' | G_{t-1}, \lambda) P(G_{t+1} | G_t = s', \lambda) P(D_t | G_t = s')}{P(G_t = s | G_{t-1}, \lambda) P(G_{t+1} | G_t = s, \lambda) P(D_t | G_t = s)}, & \text{if } t = 2, \dots, T - 1, \\ \frac{P(G_t = s' | G_{t-1}, \lambda) P(D_t | G_t = s')}{P(G_t = s | G_{t-1}, \lambda) P(D_t | G_t = s)}, & \text{if } t = T \end{cases}
 \end{aligned}$$

in which the transition probability is

$$(3.2) \quad P(G_t | G_{t-1}, \lambda) = \frac{\lambda(1 - \lambda)^{\varepsilon_t - 1}}{\sum_{\varepsilon'_t=0}^{n_e} \binom{n_e}{\varepsilon'_t} \lambda(1 - \lambda)^{\varepsilon'_t - 1}},$$

where $n_e = n(n - 1)$ is the number of all possible edges; $\varepsilon_t = \|A_t - A_{t-1}\|_1$, A_t and A_{t-1} are the adjacency matrices of network G_t and G_{t-1} , respectively. The normalising constant in equation (3.2) can be computed in advance, as long as the number of vertices is fixed.

The proposal mechanism allows the sampler to transit from the current state to any other state; the resulting Markov chain is therefore both aperiodic and irreducible. Moreover, the detailed balance condition is guaranteed by the formulation of the Hastings ratio. Therefore, the proposed structural MH algorithm is a correct MCMC sampler.

Sampling λ . The parameter λ is sampled based on the Metropolis–Hastings algorithm as well. According to Bayes’ theorem, the posterior probability of λ can be computed as follows:

$$\begin{aligned}
 (3.3) \quad P(\lambda | G_{1:T}, D_{1:T}) &\propto P(D_{1:T}, G_{1:T} | \lambda) P(\lambda) \\
 &= \pi \prod_{t=2}^T P(G_t | G_{t-1}, \lambda) \prod_{t=1}^n P(D_t | G_t),
 \end{aligned}$$

where the equality statement assumes that the prior probability follows a uniform distribution.

To constrain λ between 0 and 1, we re-parameterise λ by the sigmoid function, such that $\lambda = S(\kappa)$ where $S(\kappa) = \frac{1}{e^{-\kappa} + 1}$. Accordingly, the posterior probability of κ is scaled by the determinant of the Jacobian (in this case, the Jacobian is

a scalar):

$$(3.4) \quad \begin{aligned} P(\kappa|G_{1:T}, D_{1:T}) &= P(\lambda|G_{1:T}, D_{1:T}) \frac{\partial S(\kappa)}{\partial \kappa} \\ &= P(\lambda|G_{1:T}, D_{1:T}) S(\kappa) (1 - S(\kappa)). \end{aligned}$$

Letting $\kappa'|\kappa \sim \mathcal{N}(\kappa, \sigma)$, the acceptance ratio of proposed κ' to κ is

$$(3.5) \quad \begin{aligned} \alpha_\kappa &= \frac{P(\kappa'|G_{1:T}, D_{1:T})}{P(\kappa|G_{1:T}, D_{1:T})} \\ &= \frac{\prod_{t=2}^n P(G_t|G_{t-1}, \lambda') \frac{S(\kappa')(1 - S(\kappa'))}{S(\kappa)(1 - S(\kappa))} \frac{P(\kappa|\kappa')}{P(\kappa'|\kappa)}}{\prod_{t=2}^n P(G_t|G_{t-1}, \lambda) \frac{S(\kappa)(1 - S(\kappa))}{S(\kappa')(1 - S(\kappa'))} \frac{P(\kappa|\kappa')}{P(\kappa'|\kappa)}} \\ &= \frac{\prod_{t=2}^n P(G_t|G_{t-1}, \lambda') \frac{S(\kappa')(1 - S(\kappa'))}{S(\kappa)(1 - S(\kappa))}}{\prod_{t=2}^n P(G_t|G_{t-1}, \lambda) \frac{S(\kappa)(1 - S(\kappa))}{S(\kappa')(1 - S(\kappa'))}}. \end{aligned}$$

The complete sampling algorithm is described by the following pseudocode (Algorithm 1).

Algorithm 1 MCMC sampling algorithm for HM-NEMs

Input: $\mathcal{D}, \mathcal{G}^{(0)}, \lambda^{(0)}, \kappa^{(0)} = L(\lambda^{(0)}), \sigma$ $\triangleright L(\cdot)$ is the logit function

- 1: **for** $i = 1 \rightarrow N$ **do**
- 2: **for** $t = 1 \rightarrow T$ **do**
- 3: Propose G_t^* by randomly flipping an edge in $G_t^{(i-1)}$
- 4: Compute acceptance ratio $\alpha_{G_t}^{(i)}$ with equation (3.1)
- 5: Draw $u_{G_t}^{(i)} \sim \text{Uniform}[0, 1]$
- 6: **if** $u_{G_t}^{(i)} < \alpha_{G_t}^{(i)}$ **then**
- 7: Set $G_t^{(i)} = G_t^*$
- 8: **else**
- 9: Set $G_t^{(i)} = G_t^{(i-1)}$
- 10: **end if**
- 11: **end for**
- 12: Propose κ^* from $\mathcal{N}(\kappa, \sigma)$
- 13: Compute acceptance ratio $\alpha_\kappa^{(i)}$ with equation (3.5)
- 14: Draw $u_\kappa^{(i)} \sim \text{Uniform}[0, 1]$
- 15: **if** $u_\kappa^{(i)} < \alpha_\kappa^{(i)}$ **then**
- 16: Set $\kappa^{(i)} = \kappa^*$
- 17: **else**
- 18: Set $\kappa^{(i)} = \kappa^{(i-1)}$
- 19: **end if**
- 20: $\lambda^{(i)} = S(\kappa^{(i)})$ $\triangleright S(\cdot)$ is the sigmoid function
- 21: **end for**

Expected network. Let $\mathcal{A} := \{A_t\}_1^T$ be the adjacency matrices of \mathcal{G} . The expected time-varying network $E[\mathcal{A}] = \{E[A_t]\}_1^T$ is computed by averaging over all adjacency matrices of \mathcal{G} in the estimated posterior distribution obtained from the sampling result:

$$(3.6) \quad E[A_t] = \sum_{A_t} A_t P(A_t | D_{1:T}) = \frac{1}{N - N_b} \sum_{i=1}^{N-N_b} A_t^{(i)},$$

where N_b is the number of burn-in samples and N is the total number of samples.

4. Simulation studies. To evaluate the performance of the proposed MCMC sampling algorithm for HM-NEMs, we conducted simulation studies on *in silico* data generated from artificially constructed networks. Each perturbation data set is simulated by the following steps:

1. For a given number of pathway components n , for the first time frame we randomly flip 10% off-diagonal entries of a zero adjacency matrix to generate a directed graph. This step is repeated until the graph is transitively closed.²
2. For $t = 2, 3, \dots, T$, the network state at time t is generated by transiting the previous state at time $t - 1$. In detail, we transit the previous network by flipping a random number of off-diagonal entries n_{er} following the distribution $\binom{n_e}{n_{er}} \lambda (1 - \lambda)^{n_{er}-1}$. This step is also repeated until the graph generated for time frame t is transitively closed.
3. For a network at each time frame, attach n_r reporter genes to each pathway component. For each component, generate perturbation data which are 1s standing for downstream effects and 0s for noneffects. The perturbation data are duplicated for n_p times to model biological replicates.
4. Add false negatives and false positives to the data generated in the above steps by randomly flipping α (%) true negatives and β (%) true positives.

4.1. Convergence diagnosis. To diagnose the convergence of proposed algorithm on networks that transit states rapidly, moderately and slowly, respectively, we did three simulations where λ was set to 0.1, 0.5 and 0.9. These values allow different dynamics in network evolving. Specifically, they generate fast, moderate and slow varying networks, respectively. The other parameters were fixed to $n = 6$, $n_r = 4$, $T = 8$, $n_p = 3$, $\alpha = 0.1$ and $\beta = 0.1$. It should be noted here that these parameters are set according to a sophisticated biological application to embryonic stem cells, where six genes were perturbed following phenotyping screening over eight days. For each simulation, a time varying network and corresponding perturbation data were generated according to the above protocol. Twenty independent

²Here we generate transitively closed graphs for the convenience to simulate data from NEMs. HM-NEMs, however, do not constrain the networks in the transitively closed graph space.

TABLE 1
Performance of λ estimation

	$\lambda = 0.1$	$\lambda = 0.5$	$\lambda = 0.9$
σ	2	0.65	0.65
Posterior mean	0.11	0.49	0.92
Effective sample size	4855	1301	4121
Rejection rate	0.53	0.53	0.54
Time (sec)	631.51	635.47	602.99

runs of MCMC inference were performed on each data set over 52,000 iterations to infer the network and estimate λ . In principle, the posterior can always be estimated with only one chain given that the chain is sufficiently long. The main purpose of using 20 runs in the simulation studies and the following real biological applications is to compute the Gelman and Rubin diagnostic to inspect convergence. Furthermore, with multiple runs the posterior can be estimated within a short time. The first 2000 samples of each run were treated as the burn-in period.

We first investigate the performance of λ estimation. To achieve a good rejection rate ($\sim 55\%$) according to the efficient Metropolis jumping rules [Gelman, Roberts and Gilks (1996)], we tuned σ , which is the standard deviation of the Gaussian proposal distribution (Table 1). As shown in Figure 3, the posterior distributions can be faithfully captured by our sampling algorithm. As expected, the posterior means of estimated λ are very close to their corresponding true parameters (Table 1). To assess the efficiency of sampling, we also compared the effective sample sizes across three simulations (Table 1). To further evaluate the time of convergence to stationary distributions, we computed the $\sqrt{\hat{R}}$ statistic [proposed by Gelman and Rubin (1992)]. The time consumption (per run), using R on an Intel Xeon W3520 Quad-Core 2.67 GHZ with 8 GB RAM computer, does not show a big difference between these three simulations (Table 1). We found that for all three simulations, our algorithm converged within 52,000 iterations [Figure 3(G), (H) and (I)].

Visualising the posterior distribution of state path is difficult. Instead, we evaluate the estimated distribution of the log joint likelihood. As shown in Figure 4, multiple peaks appear in the estimated log joint likelihood distribution for $\lambda = 0.9$, which indicates multiple optimal state paths. Although in all three simulations the log joint likelihood converge very quickly [as shown in Figure 4(G), (H) and (I)], it may become challenging for the algorithm to converge when there are many more optima.

To evaluate the performance of network inference, we computed expected networks using equation (3.6). Since here twenty independent runs were performed for each λ , the overall expected network is averaged over the expected networks of all runs. The adjacency matrices of these overall expected networks are illustrated

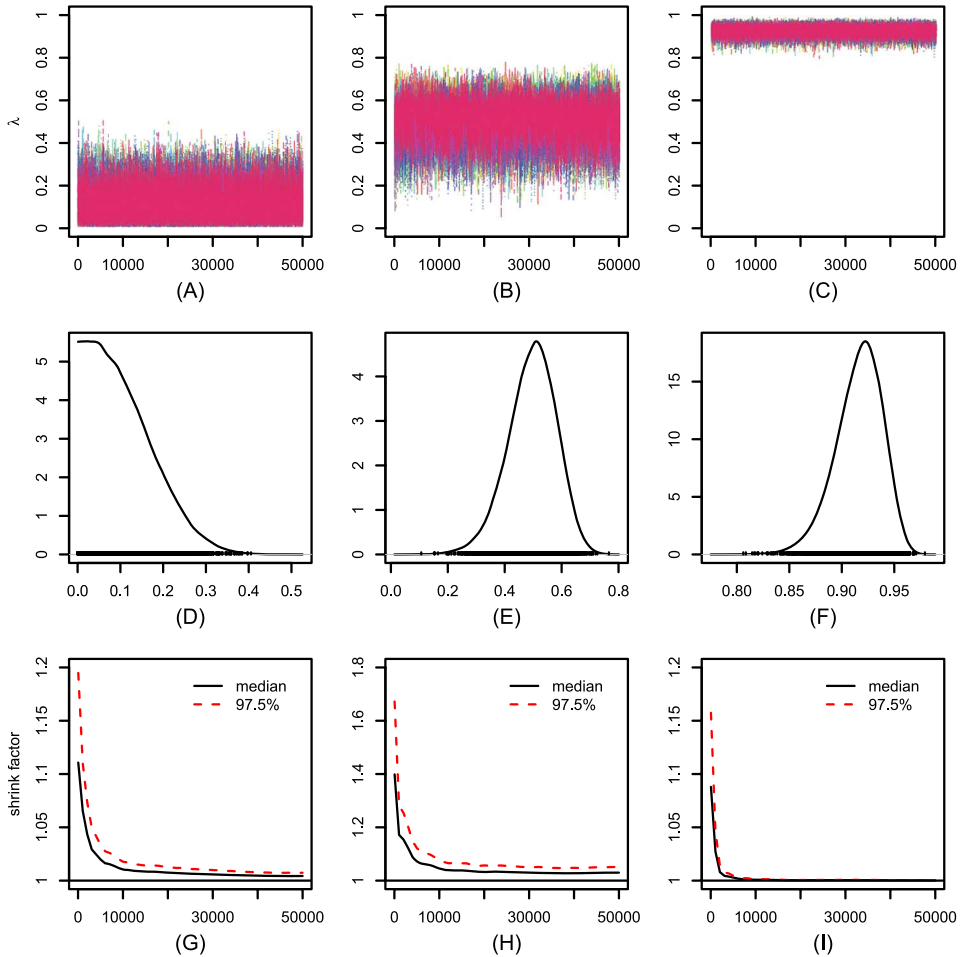


FIG. 3. Estimation and convergence diagnosis of λ . (A), (B) and (C) are trace plots, (D), (E) and (F) are estimated distributions, and (G), (H) and (I) illustrate logarithm $\sqrt{\hat{R}}$ statistics for $\lambda = 0.1$, $\lambda = 0.5$, $\lambda = 0.9$, respectively. Convergence is suggested when $\sqrt{\hat{R}}$ is close to 1.

by heatmaps in Figure 5. Indeed, the inferred networks seem to transit very dramatically for $\lambda = 0.1$, moderately for $\lambda = 0.5$ and very slowly for $\lambda = 0.9$. Moreover, considering 0.5 as a cutoff to binarise these expected networks, we can compare to the true networks generated. In all three simulations, our algorithm achieved 100% high sensitivities and 100% specificities (Table 2).³

³The sensitivity, specificity and accuracy are computed by $TP/(TP + FN)$, $TN/(TN + FP)$ and $TP + TN/(TP + FN + TN + FP)$, where TP, TN, FP, FN are the number of true positive, true negative, false positive and false negative directed edges, respectively.

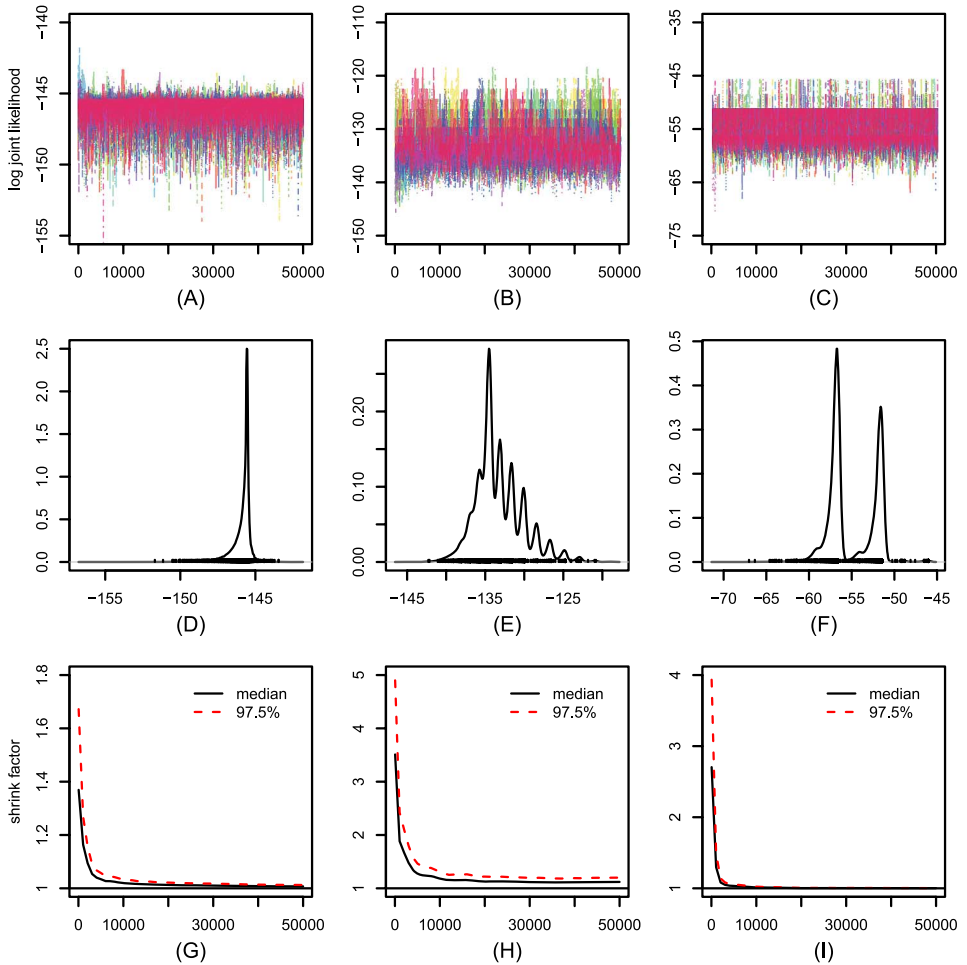


FIG. 4. Estimation and convergence diagnosis of log joint likelihood. (A), (B) and (C) are trace plots, (D), (E) and (F) are estimated distributions, and (G), (H) and (I) illustrate logarithm $\sqrt{\hat{R}}$ statistics for $\lambda = 0.1$, $\lambda = 0.5$, $\lambda = 0.9$, respectively.

Furthermore, we inspected the performance of HM-NEMs as a function of the interval of time sampling with an additional simulation study (details in Appendix A). We found that a smaller time interval tends to give a better estimation of λ and network (Figure 13).

In summary, the simulations from our model demonstrate the potential of our sampling algorithm to infer evolving networks and “smoothness” under a wide spectrum of network dynamics.

4.2. Sensitivity analysis. To assess the influence of several main factors, λ and the error probabilities α and β to the performance of our algorithm, we vary α and

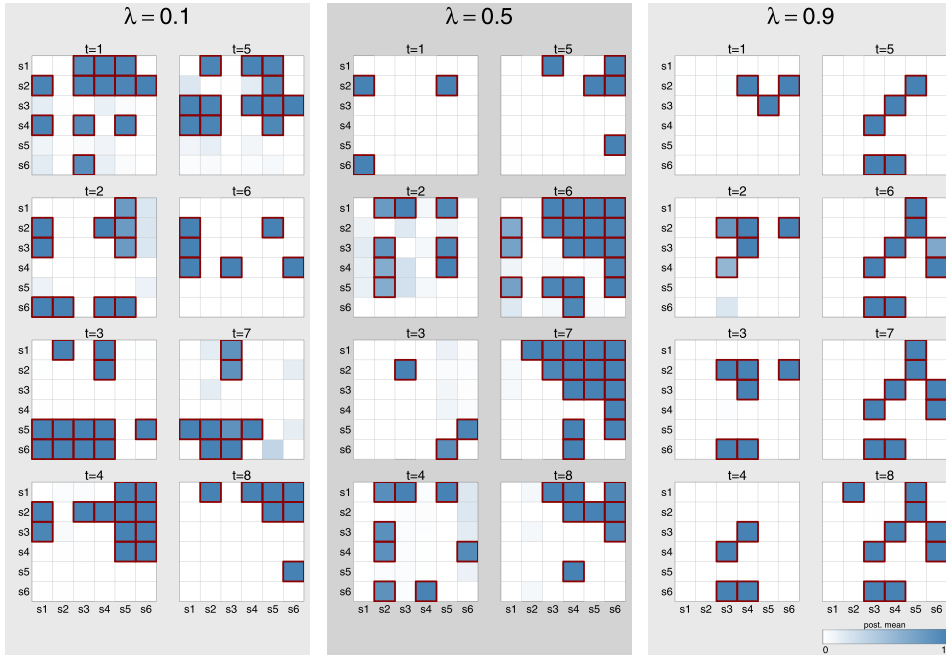


FIG. 5. Expected networks in simulation studies. The left, middle and right panels correspond to $\lambda = 0.1, 0.5$ and 0.9 , simulating networks that transit quickly, moderately and slowly, respectively. Each heatmap illustrates the posterior means of edges directed from pathway components in rows to their counterparts in columns. The directed edges of true networks are outlined with bold borders in red.

β from 0.1 to 0.5 to simulate artificial data sets for the three networks (corresponding to $\lambda = 0.1, 0.5$ and 0.9 , resp.) we have already generated in Section 4.1. For each combination of parameters (λ, α and β), we simulated 1000 random data sets and performed MCMC sampling over 12,000 iterations, which are sufficient for the algorithm to converge according to Figures 3 and 4, with the first 2000 as the burn-in period. The mean Monte Carlo errors of estimated λ and the accuracies (footnote 3 in Section 4.1) of expected networks binarised with a cutoff of 0.5 were calculated for each parameter setting.

TABLE 2
Performance of network inference

	$\lambda = 0.1$	$\lambda = 0.5$	$\lambda = 0.9$
Sensitivity	100%	100%	100%
Specificity	100%	100%	100%

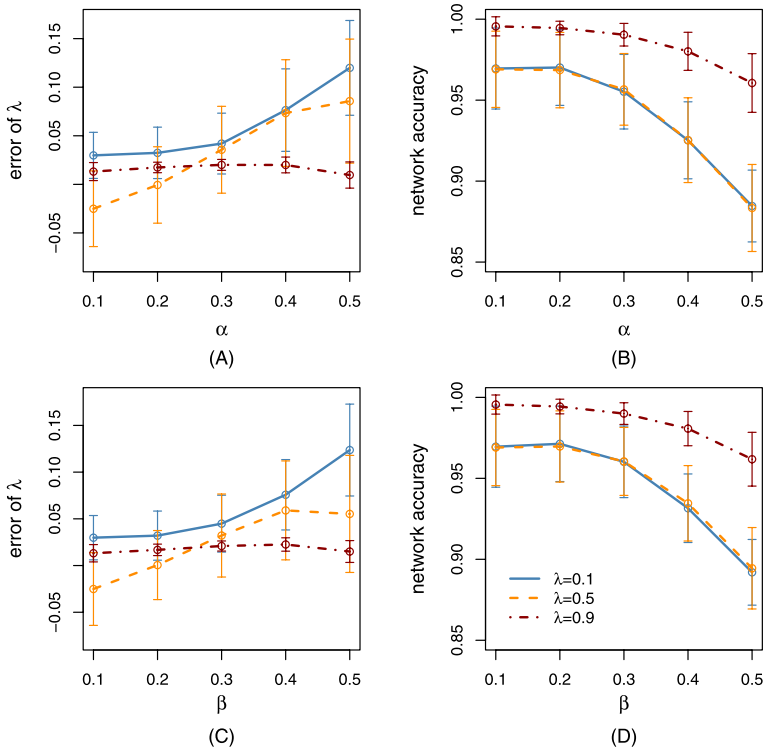


FIG. 6. Mean Monte Carlo errors of estimated λ [(A) and (C)] and accuracies of inferred expected networks [(B) and (D)] as a function of α (when $\beta = 0.1$) and β (when $\alpha = 0.1$). Lines colored in blue, orange and red correspond to $\lambda = 0.1, 0.5$ and 0.9 , respectively. Error bars indicate one standard deviation of the mean.

As shown in Figure 6, α and β affect more the performance on networks that transit relatively fast ($\lambda = 0.1$ and 0.5) than those that transit slowly ($\lambda = 0.9$), indicating that our algorithm is more robust to data noise in smooth networks. Nevertheless, no matter how λ varies, our algorithm can still achieve very promising performance (mean Monte Carlo error of $\lambda < 0.05$ and accuracy of inferred network > 0.95) when α and β are $\leq 30\%$, which is easily satisfied in real biological experiments.

We further used ANOVA to quantify the relative contributions of α , β and λ to the performance of our algorithm. Table 3 combines the results of a design-based ANOVA of the mean Monte Carlo error of estimated λ and the accuracy of inferred networks. As expected, all factors and their interactions are very significantly associated with performance ($p < 0.0001$). Interestingly, λ itself explains 30.41% total variation of the mean Monte Carlo error of estimated λ , which is much more than the 8.21% and 8.54% explained by α and β , indicating that λ estimation is more sensitive to the smoothness of networks. However, network inference is more

TABLE 3

Analysis of variance of mean Monte Carlo errors of estimated λ and accuracies of inferred networks. All factors and interactions were statistically significant with $p < 0.0001$

	Df	Mean error of λ		Network accuracy	
		Sum Sq	F-value	Sum Sq	F-value
λ	2	762.32	246,560.81	41.54	37,650.57
α	4	205.90	33,296.87	447.53	202,801.65
β	4	214.02	34,609.80	425.06	192,617.84
$\lambda : \alpha$	8	365.01	29,514.12	1.23	278.97
$\lambda : \beta$	8	361.83	29,257.05	0.80	181.54
$\alpha : \beta$	16	331.15	13,388.17	138.11	15,645.82
$\lambda : \alpha : \beta$	32	150.69	3046.12	10.76	609.39
Residuals	74,925	115.83		41.34	

affected by noise in the perturbation data, as α , β and their interaction account for 91.35% total variation.

Taken together, these sensitivity analysis results demonstrate that our sampling algorithm can be reliably employed to infer evolving networks and estimate the smoothness for perturbation data that are not extremely noisy.

4.3. Coverage analysis. We next investigated the frequentist coverage of Bayesian confidence intervals as a function of α and β in different contexts of network transition. For each combination of parameter α (0.1 to 0.5), β (0.1 to 0.5) and λ (0.1, 0.5 and 0.9), we computed highest posterior density (HPD) intervals with 95% nominal coverage probability for estimated λ and log joint likelihood. The “actual” coverage probability was subsequently computed by the proportion of the time that the HPD interval contains the true λ or log joint likelihood.

As illustrated in Figure 7, the “actual” coverage probability faithfully matches the nominal coverage probability across all α and β when $\lambda = 0.1$ and 0.5. When $\lambda = 0.9$, the true λ and log joint likelihood are both outside of the Bayesian intervals when α and β are both unreasonably high (≥ 0.4). However, even when α or β are as high as 0.3, we still observed very good coverage for $\lambda = 0.9$ (Figure 14 in Appendix B).

Taken together, the coverage analysis results demonstrate that our algorithm provides good coverage performance as long as the quality of perturbation data is not extremely bad ($\alpha \leq 0.3$ and $\beta \leq 0.3$), which is often satisfied in real biological experiments.

5. Applications.

5.1. Application to neutrophil polarisation. Neutrophils are phagocytic immune cells that can detect and kill bacteria very quickly. Underlying the rapid

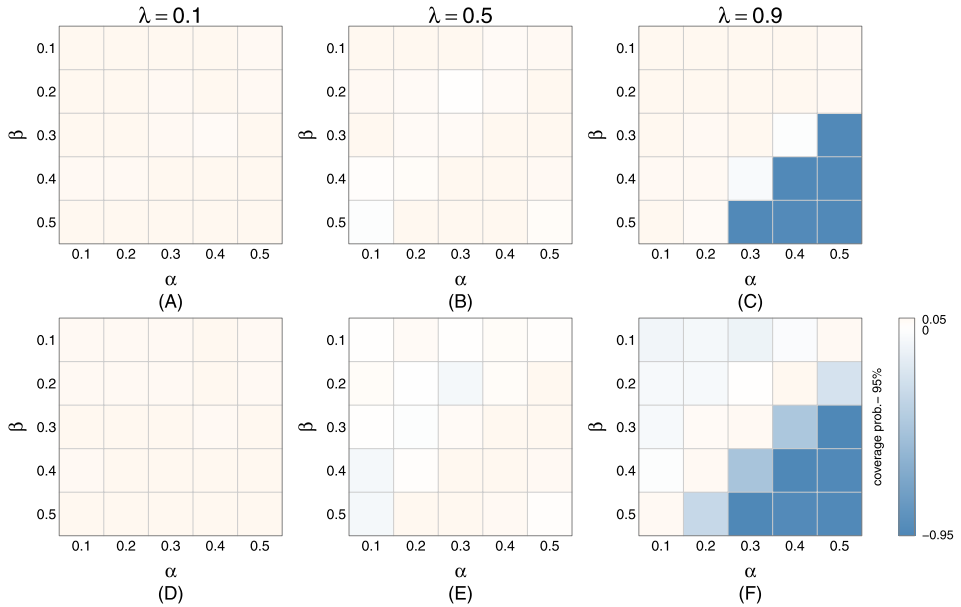


FIG. 7. Coverage as a function of α and β . (A), (B) and (C) are heatmaps illustrating the difference between coverage probability and 95% nominal coverage probability of estimated λ across different α , β and λ . Similarly, (D), (E) and (F) correspond to coverage of the log joint likelihood.

response of neutrophils to chemoattractants is the neutrophil polarity network, which upon stimulation progresses through three phases: instantaneous initiation, 2–3 min development and 10 min maintenance before adapting. Three spatially and molecularly distinct cytoskeletal modules—front (F), back (B) and microtubule (M) modules—have been implicated to be involved in the neutrophil polarity network [Small et al. (2002)]. Despite various interactions identified between these three modules, how they crosstalk dynamically to regulate polarisation is still poorly understood.

To gain mechanistic insights to the interactions between the front, back and microtubule modules over time upon stimulation, Ku et al. (2012) conducted systematic pharmacological perturbations to the three modules and employed a microscopy-based approach to quantify neutrophil polarisation phenotypes. In detail, each module was targeted by two opposing mechanistically distinct drugs: LasA (inhibitor) and Jas (enhancer) for the F module, Y27632 (inhibitor) and Calp (enhancer) for the B module, Noco (inhibitor) and Taxol (enhancer) for the M module. Each perturbation experiment was done with 2 to 6 replicates over 600 seconds after stimulation of f-Met-Leu-Phe (fMLP), which is a strong chemoattractant directing movements of neutrophils towards bacteria. As a control, responses of neutrophils to fMLP without drug treatment were also investigated in 20 replicates. The perturbation effect of the three modules was monitored by three protein markers: F-actin for the F module, α -tubulin for the M module, and

p-MLC2 for the B module, respectively. For each protein marker, intensity and polarity were quantified based on image analysis. In this application the pathway components are the three perturbed modules (F, B and M), while effect reporters are the three biochemical markers (F-actin, p-MLC2 and α -tubulin).

In the perturbation experiments, cells were fixed at 11 nonuniform time points from 0 to 600 seconds. The original time series were interpolated and smoothed to generate a response curve for each replicate, perturbation, protein marker and phenotype [details in Ku et al. (2012)]. Without loss of generality, here we focus on the interpolated polarisation response data of perturbation by enhancers of Jas, Calp and Taxol across 41 time points with the same sampling interval of 15 seconds.

At time point t for perturbation k , a t -score was computed by comparing the observed phenotype i with the reference distribution of phenotypes in control experiments. The t -value was used to compute the probability (p_{ikt}) that the perturbation phenotype is different from controls based on one sample Bayesian t -test [Rouder et al. (2009)]. As the relationships between the three modules (F, B and M) and the effect reporters (F-actin, p-MLC2 and α -tubulin) are already known, we use equation (2.3) to calculate the emission probability $P(D_t|G_t)$, which can be written as $P(d_{ikt}|G_t) = p_{ikt}$ if $S_{jkt} = 1$ and $P(d_{ikt}|G_t) = 1 - p_{ikt}$ if $S_{jkt} = 0$. Having obtained the probabilities for all phenotypes, perturbations and time points, we applied HM-NEMs to infer the dynamic interplay between the F, B and M modules.

Twenty parallel runs of MCMC sampling were performed to do parameter estimation and network inference. Each sampling was run for 22,000 iterations, and the first 2000 were considered as the burn-in period. As shown in Figure 8, we observed a very fast convergence for both λ and the log joint likelihood. The posterior mean of λ is ~ 0.95 , indicating that the polarity network of neutrophils progresses very smoothly.

The overall expected network was summarised over all twenty parallel chains, and the snapshots at every 60 seconds are illustrated in the heatmaps of Figure 9. The vast majority of the posterior means of pairwise interactions are either close to 1 or 0, suggesting that the signalling interactions can be identified by our algorithm without ambiguity. The overall expected network was further binarised based on a cutoff of posterior mean at 0.5 (Figure 9). Intriguingly, the feedforward signalling of M module to B and F modules dominates the maintenance phase (180 to 600 sec), which is consistent with the persistent crosstalks identified in Ku et al. (2012) using a z -score-based approach. Signalling interactions inferred at early stages (0 \sim 120 sec), mainly from the back and front modules to the microtubule module, coincide with the transient crosstalks, which are known to happen during the initiation and development phases of neutrophil polarisation. Taken together, the evolving network inferred by HM-NEMs captures dynamic crosstalks between the front, back and microtubule modules underlying neutrophil polarisation.

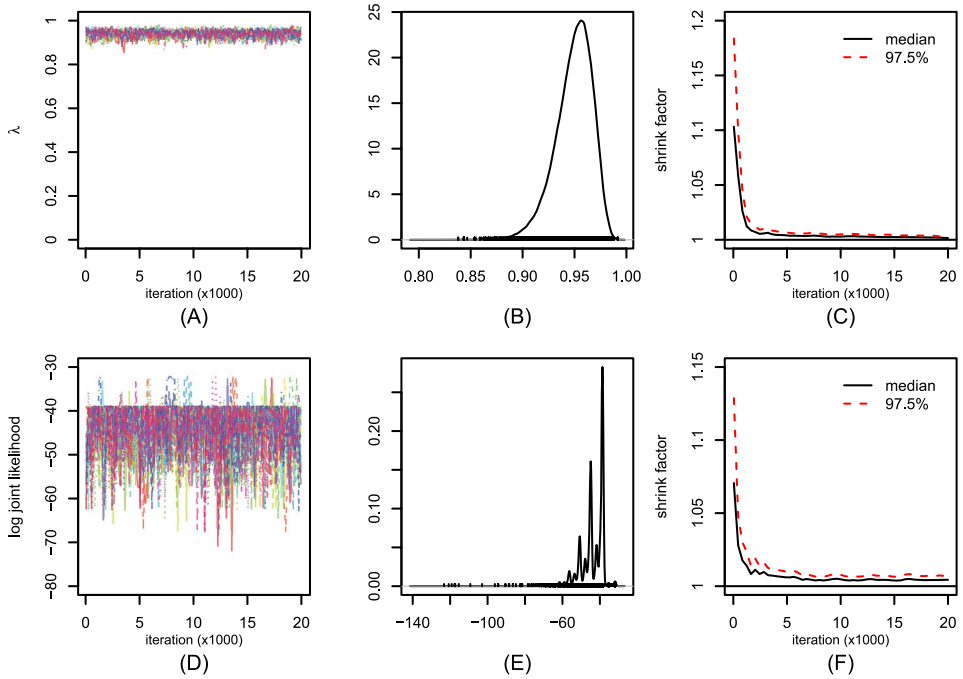


FIG. 8. *Parameter estimation and convergence diagnosis in the application to neutrophil polarisation. (A), (B) and (C) are trace plot, posterior distribution and logarithm $\sqrt{\hat{R}}$ statistics for λ estimation. (D), (E) and (F) are trace plot, posterior distribution and logarithm $\sqrt{\hat{R}}$ statistics for the log joint likelihood estimation.*

5.2. *Application to mouse embryonic stem cells.* There has been a wealth of studies on the self-renewal and differentiation mechanisms of embryonic stem cells (ESCs) for decades. [Ivanova et al. \(2006\)](#) conducted an integrated approach to reveal potential regulators participating in the self-renewal process of murine ES cells. They first used shRNAs (short hairpin RNAs) to knock down potential transcription factors and identified six regulators (*Nanog*, *Oct4*, *Sox2*, *Esrrb*, *Tbx3* and *Tcl1*). Transcriptome dynamics were subsequently monitored after perturbation of each of these six factors over eight days using microarrays. Using a simple clustering analysis, they found that the six regulators are involved in two global pathways regulating ESC self-renewal [[Ivanova et al. \(2006\)](#)]. However, how these identified factors interact with each other remains unclear. Here, we attempt to address this challenge by HM-NEMs.

The raw gene expression data were preprocessed and discretised following the same strategy in [Anchang et al. \(2009\)](#). From the discretised perturbation data, we applied HM-NEMs to reconstruct the ESC self-renewal network. Twenty independent runs of MCMC sampling were performed over 202,000 iterations including the first 2000 burn-in period. To speed up convergence, the starting network at

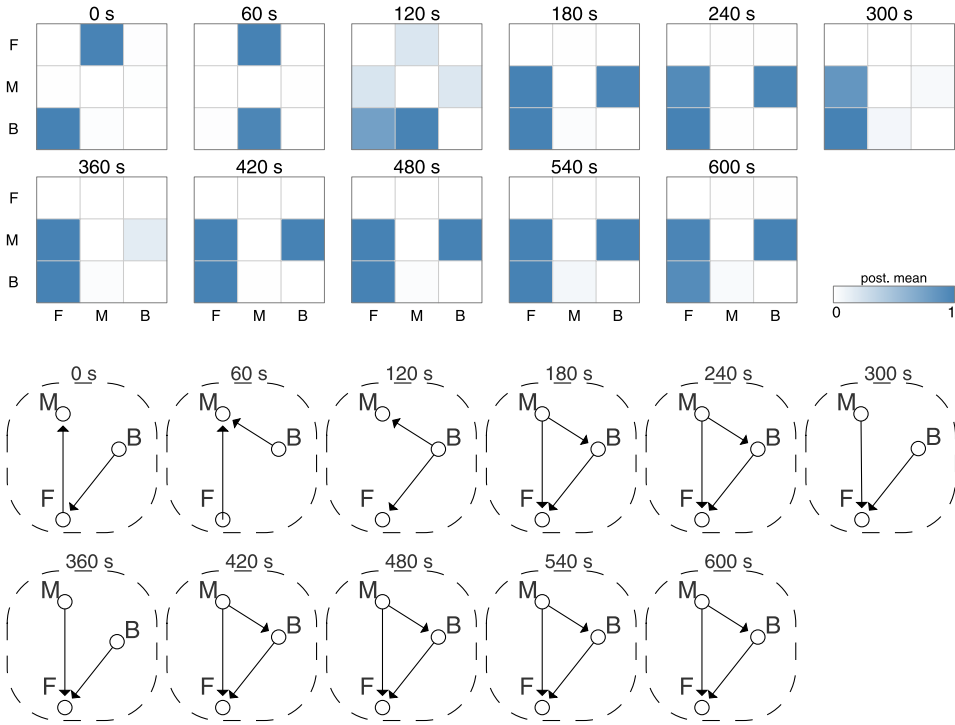


FIG. 9. Expected (upper panel) and discretised (lower panel) neutrophil polarisation network. The evolving network identified by HM-NEMs precisely captures the three-phase progression of the polarity network of neutrophils: polarisation initiation (0 sec), polarisation development (60 to 120 sec) and polarisation maintenance (180 to 600 sec). The discretised network was produced by R package *Reder* [Castro et al. (2012)].

each time point was inferred by static NEMs with a greedy hill-climbing algorithm [Markowitz (2006)]. As shown in Figure 10, the Markov chains of λ and log joint likelihood converge very quickly. Similar to the neutrophil polarisation network, the posterior mean of estimated λ is ~ 0.88 , suggesting that the network transition underlying ESC early differentiation is also very smooth.

We computed the overall expected network across all twenty chains, and observed that the vast majority of signalling interactions between the six regulators are quite deterministic (illustrated by the heatmaps in Figure 11). Using a cut-off of posterior mean at 0.5, we further discretised the overall expected network (Figure 11). Interestingly, the network suggests both feed-forward and feedback regulations during early differentiation of ESCs. One feed-forward loop (day 4 to day 8) is found between *Sox2*, *Oct4* and *Tcl1*, which can be validated by the transcriptional regulations of *Sox2* on *Oct4* [Masui et al. (2007)] and *Oct4* on *Tcl1* [Matoba et al. (2006)]. Another feed-forward loop (day 4 to day 8) is between *Tbx3*, *Esrrb* and *Tcl1*, which is less characterised in the literature. However,

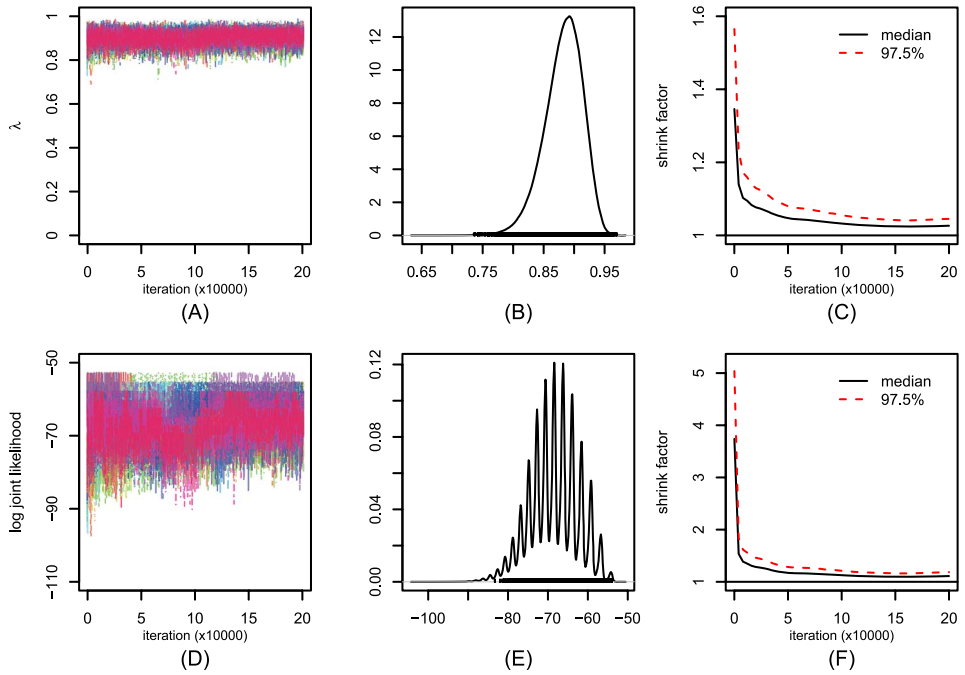


FIG. 10. *Parameter estimation and convergence diagnosis in the application to mouse embryonic stem cells. (A), (B) and (C) are trace plot, posterior distribution and logarithm $\sqrt{\hat{R}}$ statistics for λ estimation. (D), (E) and (F) are trace plot, posterior distribution and logarithm $\sqrt{\hat{R}}$ statistics for the log joint likelihood estimation.*

the network constituted by them is found to be critical to block the differentiation into epiblast-derived lineages [Ivanova et al. (2006)]. These two feed-forward loops are mainly regulating the expression of *Tcl1*, which was shown to be important for ESC proliferation but not differentiation [Matoba et al. (2006), Ivanova et al. (2006)].

Feedback interactions are mainly found between *Nanog* and *Oct4/Sox2* and *Tbx3/Esrrb*. *Nanog* is found downstream of *Sox2/Oct4* during the early stage (day 1 to day 3), but upstream of *Oct4* and/or *Sox2* after day 4. The feedback regulations between *Nanog* and *Sox2/Oct4* are known to be critical for maintaining the pluripotency of ESCs [Loh et al. (2006)]. *Nanog* can bind to the promoter regions of *Oct4* and *Sox2*, while the *Oct4-Sox2* heterodimer can also bind to the promoter region of *Nanog* [Boyer et al. (2005), Loh et al. (2006)]. Thus, the feedback between *Nanog* and *Sox2/Oct4* may occur at the transcription level. The feedback regulations between *Nanog* and *Tbx3/Esrrb* are also implicated in the literature. *Nanog* is known to positively regulate expression of *Esrrb*, while *Tbx3* and *Esrrb* can also enhance *Nanog* expression [Loh et al. (2006), van den Berg et al. (2008), Niwa et al. (2009)].

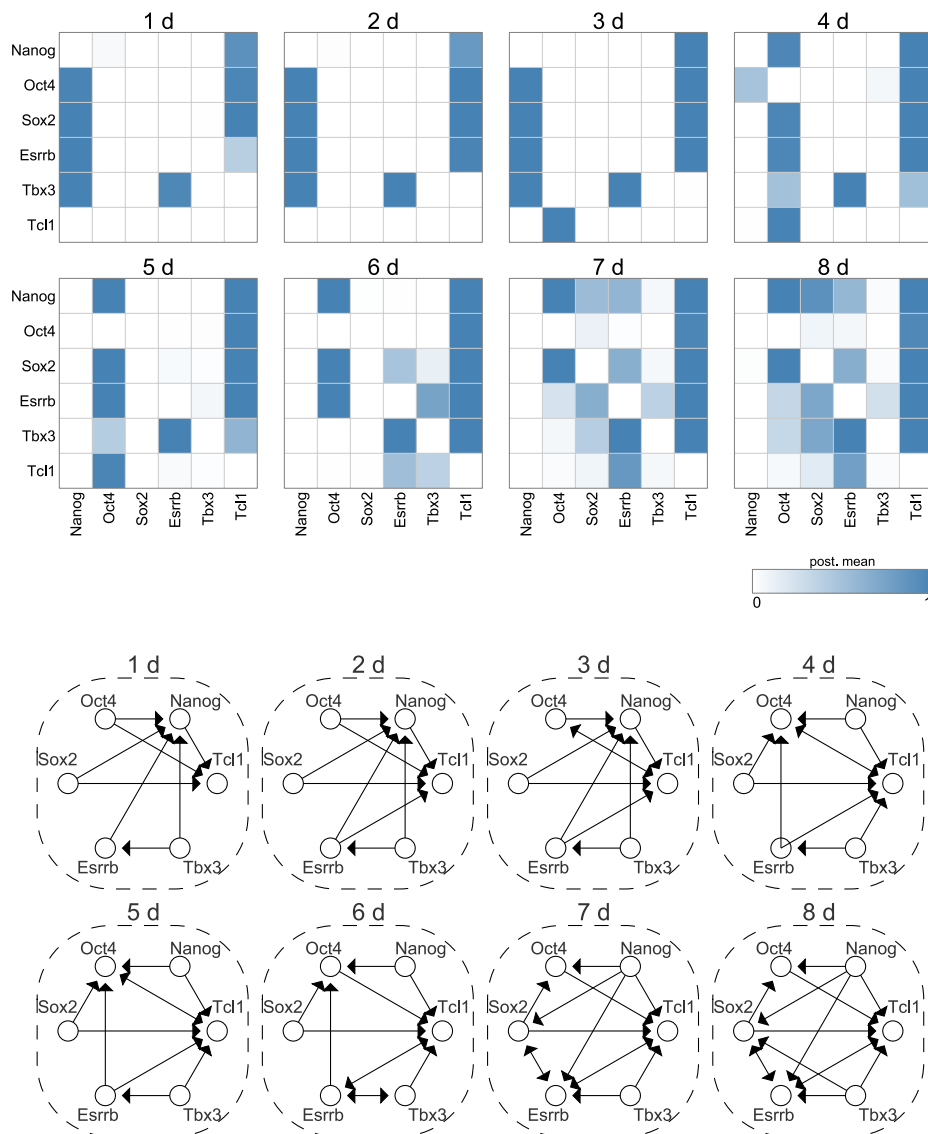


FIG. 11. *Expected (upper panel) and discretised (lower panel) network in the application to mouse embryonic stem cells. The network identified by HM-NEMS suggests that the feedback regulations between Nanog, Sox2 and Oct4 may underlie early differentiation of mouse ESCs.*

Taken together, we hypothesize that the time-varying signalling network inferred by HM-NEMs underlying the early differentiation of ESCs may involve two stages. During the early stage (day 1 to day 3), *Sox2* and *Oct4* positively regulate expression of *Nanog* so that ESCs maintain its self-renewal. During the late stage (after day 4), *Nanog* starts to regulate *Oct4* and/or *Sox2* and lead ESCs

to differentiate. Our hypothesis can be confirmed in part by previous findings that high *Nanog* expression is important for ESCs to possess high self-renewal efficiency, whereas low *Nanog* expression is associated with increased differentiation propensity [Kalmar et al. (2009), Navarro et al. (2012)]. Nonetheless, biological experiments should be conducted to further validate the reconstructed network.

6. Discussion. In this paper we propose hidden Markov nested effects models for reconstructing signalling networks evolving over time. We developed a MCMC sampling algorithm to infer the most probable state path (the evolving network) while estimating the parameter λ that indicates the intrinsic feature of network evolutions. With simulations from the model, the proposed MCMC sampling algorithm was shown to work efficiently on networks under a wide spectrum of network dynamics as long as the perturbation data is not extremely noisy. We also demonstrated the model's potential to infer evolving networks underlying dynamic biological processes by two real applications.

Identifiability. Inference of NEMs is based on the model posterior, which combines the prior distributions on pathway structure and positions of effect reporters with the data on effect reporter states under perturbations. We generally choose uniform priors and, for example, the position of each effect reporter is equally likely at each pathway component. In the following, we use a toy example involving only two pathway components (Figure 12) to discuss the identifiability of NEMs. We will show that whether the two structures in the example ($A \rightarrow B$ and $B \rightarrow A$) are distinguishable or not depends on the data observed at the effect reporter E.

If a single effect reporter shows effects under both perturbations [Figure 12(a); a special case of two perturbations showing the same profile over all effect reporters], the structures $A \rightarrow B$ and $B \rightarrow A$ are indeed indistinguishable. In this symmetric case the effect reporter can always be attached to the downstream gene without preferring one structure to the other. Generally, NEMs model subset relations and in this situation the set of effects after perturbing A ($= \{E\}$) is identical to the set of effects after perturbing B ($= \{E\}$), which indeed offers no information on how to order A and B. This issue has been identified already in the first NEM papers [Markowitz, Bloch and Spang (2005), Markowitz et al. (2007)] and it is the reason why we often use bidirectional arrows to indicate pairs of pathway components with (up to noise) identical effect profiles. For larger networks we generally merge all these nodes into a joint node and, as a result, infer a hierarchy of clusters of genes, instead of a hierarchy of individual genes [Markowitz et al. (2007)].

In practice, however, this identifiability problem may not be dramatic, because effect profiles are generally not identical, especially with gene expression readout on thousands of genes like in our second case study. As the simplest example,

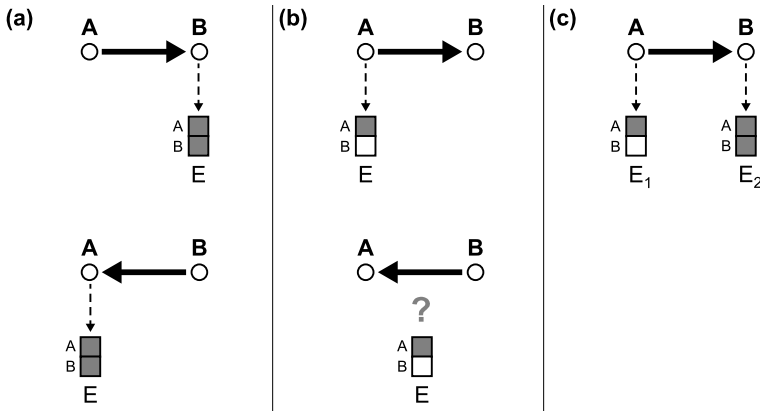


FIG. 12. NEM examples involving only two pathway components A and B. Inference success depends on the information in the data (boxes for effect reporter status under perturbation of A or B: shaded = effect; white = no effect). Dashed edges show error-free (and thus most likely) effect reporter position given the A–B structure and the data. (a) Single effect reporter showing effects under both perturbations makes structures indistinguishable; (b) single effect reporter showing effect under only one perturbation (in this case A) prefers structure where the perturbed gene is on top; (c) generally we have more than one effect reporter and this is an example of a small subset structure on two reporters.

imagine that the effect reporter only shows an effect under one perturbation (say A) but not the other [Figure 12(b)]. Even with only a single reporter, this small change in the data improves the situation drastically: now the set of effects after perturbing A ($= \{E\}$) is a superset of the set of effects after perturbing B ($= \emptyset$). Our likelihood (and also the marginal likelihood averaging over all reporter positions) now prefers the $A \rightarrow B$ structure, because it allows to attach E to A without incurring any false positive or negative effects, while no error-free attachment is possible for $B \rightarrow A$ (if we attached it to B, the reporter profile would be completely wrong; and if we attached it to A, the effect of perturbing B would still be missing).

In real applications there are usually more effect reporters than pathway components. Our scenario is thus better represented by a graph with two effect reporters [Figure 12(c)]. If both reporters show effects under both perturbations, we are back in the situation of Figure 12(a), but generally we observe patterns like the one shown here: the set of effects after perturbing A ($= \{E_1, E_2\}$) is a superset of the effects of perturbing B ($= \{E_2\}$), which allows unique identification of the A–B structure and reporter assignment.

Theoretically, it has also been proved that NEMs are identifiable for sufficiently ‘good’ data, which can be satisfied by a sufficient number of replicate measurements, and the pathway graph and the assignment of reporters to pathway components are unique up to reversals [see Theorems 1 and 3 in Tresch and Markowitz (2008)].

In HM-NEMs, the identifiability of hidden states (in our case networks, also under given parameters) is expected to be at least the same as estimating the states separately from different time points with a static model. One could see a HM-NEM as a static NEM with an informative prior estimated from different time points. In this regard, it may be easier to estimate a network at a given time point with HM-NEM than a static NEM.

Label switching. In HMMs, the label switching problem arises from the fact that the observation model is the same as the generative process in a mixture model. As the labels for each component are exchangeable, the marginal likelihood (which is the objective function for parameter estimation) after integrating out the unknown labels is invariant to permutations of parameters. When the hidden states are the parameter labels, HMMs can be seen as mixture models with a Markov prior over the labels. The marginal likelihood is again invariant to permutations of the parameters. Thus, the label switching got introduced into HMMs.

However, when the hidden states are the parameters of the distribution rather than the labels of the parameters, the situation changes. For the observation model there is only one parameter rather than K number of parameters in the marginal likelihood. Let us illustrate this with a 2-state Gaussian HMM. Assuming the same covariance matrix, at a give time point, the observation model is $N(\mu_k, \Sigma)$, $k \in (1, 2)$. Therefore, there are two unknown parameters μ_1 and μ_2 after integrating out the unknown labels. Now consider for the same observed data, but the hidden variable is μ itself. Integrating out μ , there is only Σ left in the marginal likelihood. Hence, there is nothing to switch any more. In HM-NEMs, the hidden states are the network topologies which are the parameters of NEMs rather than labels. Therefore, we think that label switching may not be a problem for HM-NEMs.

Generality. Although HM-NEMs belong to the family of structural HMMs, it is specifically tailored for indirect data from systematic perturbation screens. HM-NEMs extend classical nested effects models which infer static signalling networks. With an identity transition kernel ($\lambda \rightarrow 1$), HM-NEMs are identical to static NEMs since the graph chosen at the first time frame persists till the end. On the other hand, when $\lambda \rightarrow 0$, there is no structural dependencies between consecutive time points (the process loses its memory), and independent NEMs are fitted for each observation time point. To strike the balance between a static view of the data and the negligence of time dependence, HM-NEMs use a transition kernel to model the nature of biological networks that transit smoothly over time. Beyond the NEMs family, there are also generalisable elements in the model. Particularly, the transition probability setting could be applied to other structural HMM including DBNs.

Scalability. In HM-NEMs, the cardinality of the state space grows exponentially with the size of the signalling network. The traditional Baum–Welch algorithm for

HMM suffers from the time complexity of $O(K^2TM)$, where M is the number of the EM iterations, $K = 2^{n_s(n_s-1)}$ is the size of network state space for n_s pathway components and T is the number of time points. As the networks grow in size, the use of this type of method might be prohibited. Such a scalability problem makes MCMC particularly appealing to HM-NEMs, since the Monte Carlo estimator does not suffer the curse of dimensionality. However, a large state space may potentially lead to highly multimodal posterior or low identifiability, both of which can result in poorly mixing Markov chains.

More efficient inference methods. Both scaling and generalising HM-NEMs demand efficient inference strategies. Our inference method is an elementary single-site update Gibbs sampler. The sampler could be easily trapped in a local region of the posterior due to the fact that the hidden variables are updated sequentially. This could be solved by employing block-type update schemes which sample a part of or even the entire state path in one go. In addition, a significant efficiency gain could be obtained by sampling λ with the recently developed manifold MCMC approaches [Girolami and Calderhead (2011)]. Another improvable point is to use a better structural MCMC which efficiently explores the network topologies. To this end, one could convert the network structure into ordered space [Friedman and Koller (2003)]. Other advances in structural MCMC in DAGs, including those in Grzegorzczuk and Husmeier (2008), could be applied in our setting as well. These are the algorithmic avenues we are currently pursuing.

Biological applicability and implications. In this paper we also demonstrated the potential of HM-NEMs to gain biological insights to the network transition underlying complex dynamic biological processes. In the application to neutrophils, HM-NEMs capture the transition between initiation, development and maintenance phases during neutrophil polarisation. In another application to mouse embryonic stem cells (ESCs), the time-varying network inferred by HM-NEMs suggests that underlying early differentiation of ESCs may be the feedback regulations between *Nanog*, *Sox2* and *Oct4*. Our results on these two real biological applications are in part consistent with recent findings in the literature, and generate an intriguing hypothesis about the mechanisms of network evolution that can be tested by further experiments.

APPENDIX A: THE IMPACT OF TIME SAMPLING ON THE PERFORMANCE OF HM-NEMs

Without loss of generality, we set $\lambda = 0.9$ and generated a random evolving network of $n = 6$ pathway components over $T = 128$ time points. Setting the same parameters ($n_r = 4$ reporters per pathway component, $n_p = 3$ replicates, $\alpha = 0.1$ and $\beta = 0.1$) as the simulation study in Section 4.1, we generated an artificial perturbation data set. Next, we sampled the complete data set with the time interval

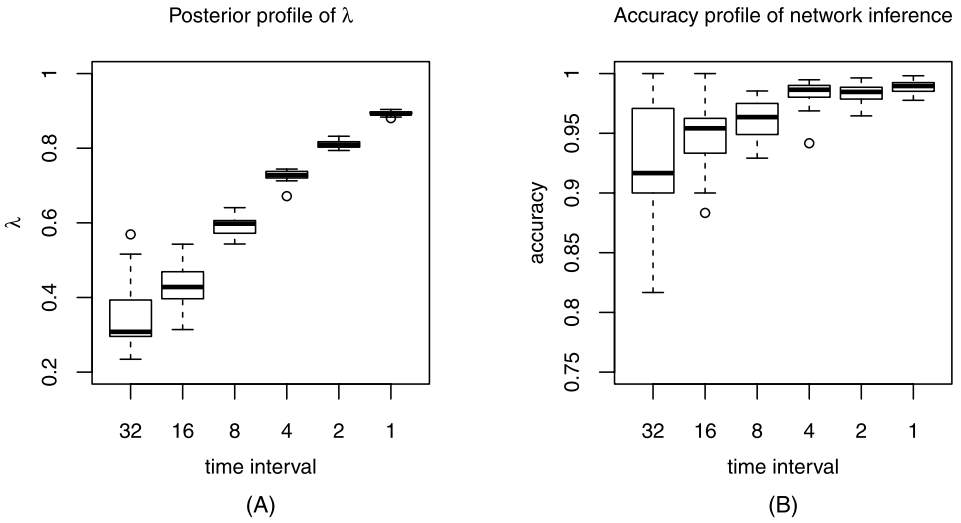


FIG. 13. (A) Posterior profile of λ , and (B) accuracy profile of network inference as a function of the interval of time sampling.

varying from 1 to 32. HM-NEMs are then applied to estimate the posterior of λ and evolving network for each setting of time sampling. As expected, the posterior mean of λ increases and approaches the real λ as time interval decreases [Figure 13(A)], indicating that a smaller time interval tends to give a “smoother” estimate of the network. The performance of network inference, assessed by accuracy, is also improved by more time samples [Figure 13(B)]. However, even for only 4 time points (time interval = 32), HM-NEMs achieved a good performance (median accuracy = 0.92).

APPENDIX B: HPD INTERVALS AS A FUNCTION OF α AND β

For each combination of parameter α , β and λ , we computed highest posterior density (HPD) intervals with 95% nominal coverage probability for estimated λ and log joint likelihood. As shown in Figure 14, HPD intervals for estimated λ and log joint likelihood both cover the true λ and likelihood even when α and β are as high as 30%, demonstrating the robustness of our algorithm to noise in observed perturbation data.

Acknowledgements. We thank Professor Steve Altschuler and Dr. Chin-Jen Ku at the University of Texas Southwestern Medical Center for kindly sharing the neutrophil perturbation data. We also thank Dr. Achim Tresch at the Max Planck Institute in Cologne and Dr. Roland F. Schwarz at the European Bioinformatics Institute for helpful discussions and commenting on drafts of the paper.

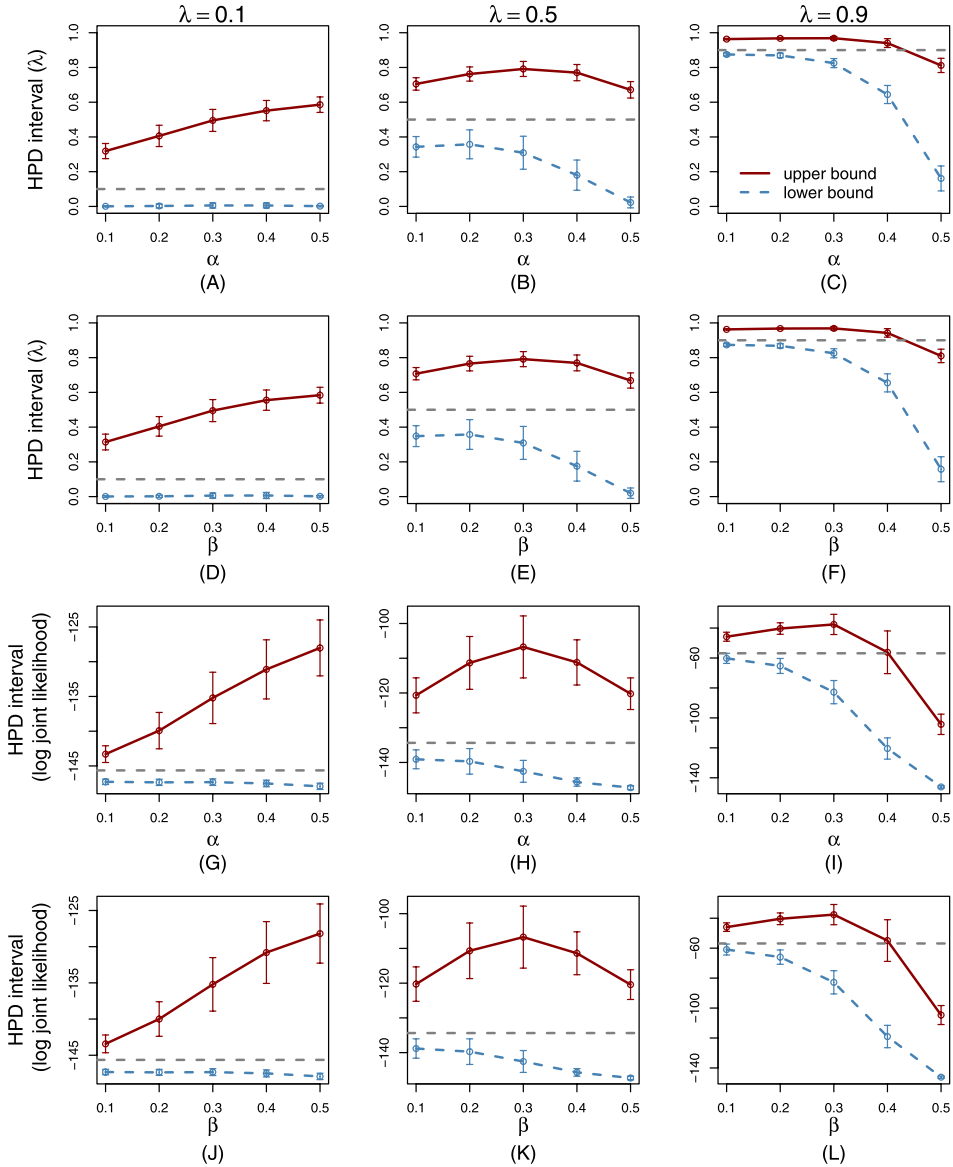


FIG. 14. HPD intervals of λ [(A) to (F)] and log joint likelihood [(G) to (L)] as a function of α (when $\beta = 0.3$) and β (when $\alpha = 0.3$). Solid red and dashed blue lines represent upper and lower confidence bounds, respectively. Error bars indicate one standard deviation of the mean. The true λ and log joint likelihood are denoted by dashed gray lines.

REFERENCES

- AHMED, A. and XING, E. P. (2009). Recovering time-varying networks of dependencies in social and biological studies. *Proc. Natl. Acad. Sci. USA* **106** 11878–11883.
- ANCHANG, B., SADEH, M. J., JACOB, J., TRESCH, A., VLAD, M. O., OEFNER, P. J. and SPANG, R. (2009). Modeling the temporal interplay of molecular signaling and gene expression by using dynamic nested effects models. *Proc. Natl. Acad. Sci. USA* **106** 6447–6452.
- BOUTROS, M. and AHRINGER, J. (2008). The art and design of genetic screens: RNA interference. *Nat. Rev. Genet.* **9** 554–566.
- BOYER, L. A., LEE, T. I., COLE, M. F., JOHNSTONE, S. E., LEVINE, S. S., ZUCKER, J. P., GUENTHER, M. G., KUMAR, R. M., MURRAY, H. L., JENNER, R. G. et al. (2005). Core transcriptional regulatory circuitry in human embryonic stem cells. *Cell* **122** 947–956.
- CASTRO, M. A., WANG, X., FLETCHER, M. N., MEYER, K. B. and MARKOWETZ, F. (2012). RedeR: R/Bioconductor package for representing modular structures, nested networks and multiple levels of hierarchical associations. *Genome Biol.* **13** R29.
- FAILMEZGER, H., PRAVEEN, P., TRESCH, A. and FRÖHLICH, H. (2013). Learning gene network structure from time laps cell imaging in RNAi Knock downs. *Bioinformatics* **29** 1534–1540.
- FRIEDMAN, N. and KOLLER, D. (2003). Being Bayesian about network structure. A Bayesian approach to structure discovery in Bayesian networks. *Machine Learning* **50** 95–125.
- FRÖHLICH, H., PRAVEEN, P. and TRESCH, A. (2011). Fast and efficient dynamic nested effects models. *Bioinformatics* **27** 238–244.
- FRÖHLICH, H., FELLMANN, M., SUELTMANN, H., POUSTKA, A. and BEISSBARTH, T. (2007). Large scale statistical inference of signaling pathways from RNAi and microarray data. *BMC Bioinformatics* **8** 386.
- FRÖHLICH, H., FELLMANN, M., SUELTMANN, H., POUSTKA, A. and BEISSBARTH, T. (2008). Estimating large-scale signaling networks through nested effect models with intervention effects from microarray data. *Bioinformatics* **24** 2650–2656.
- GELMAN, A., ROBERTS, G. O. and GILKS, W. R. (1996). Efficient Metropolis jumping rules. *Bayesian Stat.* **5** 599–607.
- GELMAN, A. and RUBIN, D. B. (1992). Inference from iterative simulation using multiple sequences. *Statist. Sci.* **7** 457–472.
- GEYER, C. (2011). Introduction to Markov chain Monte Carlo. In *Handbook of Markov Chain Monte Carlo* (S. Brooks, A. Gelman, G. Jones and X. L. Meng, eds.). CRC Press, Boca Raton, FL. MR2742422
- GIROLAMI, M. and CALDERHEAD, B. (2011). Riemann manifold Langevin and Hamiltonian Monte Carlo methods. *J. R. Stat. Soc. Ser. B Stat. Methodol.* **73** 123–214. MR2814492
- GRZEGORCZYK, M. and HUSMEIER, D. (2008). Improving the structure MCMC sampler for Bayesian networks by introducing a new edge reversal move. *Machine Learning* **71** 265–305.
- GRZEGORCZYK, M. and HUSMEIER, D. (2009). Nonstationary continuous dynamic Bayesian networks. *Advances in Neural Information Processing Systems (NIPS)* **22** 682–690.
- GUO, F., HANNEKE, S., FU, W. and XING, E. P. (2007). Recovering temporally rewiring networks: A model-based approach. In *Proceedings of the 24th International Conference on Machine Learning* 321–328. ACM, Corvallis, OR.
- HANNEKE, S. and XING, E. P. (2006). Discrete temporal models of social networks. In *Proceedings of the 2006 Conference on Statistical Network Analysis* 115–125. Springer, Berlin.
- HOUSE, C. D., VASKE, C. J., SCHWARTZ, A. M., OBIAS, V., FRANK, B., LUU, T., SARVAZAN, N., IRBY, R., STRAUSBERG, R. L., HALES, T. G., STUART, J. M. and LEE, N. H. (2010). Voltage-gated Na⁺ channel SCN5A is a key regulator of a gene transcriptional network that controls colon cancer invasion. *Cancer Res.* **70** 6957–6967.
- HUSMEIER, D., DONDELINGER, F. and LEBRE, S. (2010). Inter-time segment information sharing for nonhomogeneous dynamic Bayesian networks. *Adv. Neural Inf. Process. Syst.* **23** 901–909.

- IVANOVA, N., DOBRIN, R., LU, R. et al. (2006). Dissecting self-renewal in stem cells with RNA interference. *Nature* **442** 533–538.
- KALMAR, T., LIM, C., HAYWARD, P., MUÑOZ-DESCALZO, S., NICHOLS, J., GARCIA-OJALVO, J. and ARIAS, A. M. (2009). Regulated fluctuations in Nanog expression mediate cell fate decisions in embryonic stem cells. *PLoS Biology* **7** e1000149.
- KU, C.-J., WANG, Y., WEINER, O. D., ALTSCHULER, S. J. and WU, L. F. (2012). Network crosstalk dynamically changes during neutrophil polarization. *Cell* **149** 1073–1083.
- LÈBRE, S. (2007). Stochastic process analysis for Genomics and Dynamic Bayesian Networks inference. Ph.D. thesis, Univ. d'Évry Val-d'Essonne, France.
- LOH, Y.-H., WU, Q., CHEW, J.-L., VEGA, V. B., ZHANG, W., CHEN, X., BOURQUE, G., GEORGE, J., LEONG, B., LIU, J. et al. (2006). The Oct4 and Nanog transcription network regulates pluripotency in mouse embryonic stem cells. *Nat. Genet.* **38** 431–440.
- MADIGAN, D., YORK, J. and ALLARD, D. (1995). Bayesian graphical models for discrete data. *International Statistical Review/Revue Internationale de Statistique* **63** 215–232.
- MARKOWETZ, F. (2006). Probabilistic models for gene silencing data. Ph.D. thesis, Free Univ. Berlin, Germany.
- MARKOWETZ, F. (2010). How to understand the cell by breaking it: Network analysis of gene perturbation screens. *PLoS Comput. Biol.* **6** e1000655.
- MARKOWETZ, F., BLOCH, J. and SPANG, R. (2005). Nontranscriptional pathway features reconstructed from secondary effects of RNA interference. *Bioinformatics* **21** 4026–4032.
- MARKOWETZ, F., KOSTKA, D., TROYANSKAYA, O. G. and SPANG, R. (2007). Nested effects models for high-dimensional phenotyping screens. *Bioinformatics* **23** i305–i312.
- MASUI, S., NAKATAKE, Y., TOYOOKA, Y. et al. (2007). Pluripotency governed by Sox2 via regulation of Oct3/4 expression in mouse embryonic stem cells. *Nat. Cell Biol.* **9** 625–635.
- MATOBA, R., NIWA, H., MASUI, S., OHTSUKA, S., CARTER, M. G., SHAROV, A. A. and KO, M. S. (2006). Dissecting Oct3/4-regulated gene networks in embryonic stem cells by expression profiling. *PLoS One* **1** e26.
- MURPHY, K. P. (2002). Dynamic Bayesian networks: Representation, inference and learning. Ph.D. thesis, Univ. California.
- NAVARRO, P., FESTUCCIA, N., COLBY, D., GAGLIARDI, A., MULLIN, N. P., ZHANG, W., KARWACKI-NEISIUS, V., OSORNO, R., KELLY, D., ROBERTSON, M. et al. (2012). OCT4/SOX2-independent Nanog autorepression modulates heterogeneous Nanog gene expression in mouse ES cells. *The EMBO Journal* **31** 4547–4562.
- NEUMANN, B., WALTER, T., JEAN-KARIM, H. et al. (2010). Phenotypic profiling of the human genome by time-lapse microscopy reveals cell division genes. *Nature* **464** 721–727.
- NIEDERBERGER, T., ETZOLD, S., LIDSCHREIBER, M., MAIER, K. C., MARTIN, D. E., FRÖHLICH, H., CRAMER, P. and TRESCH, A. (2012). MC EMiNEM maps the interaction landscape of the Mediator. *PLoS Comput. Biol.* **8** e1002568.
- NIWA, H., OGAWA, K., SHIMOSATO, D. and ADACHI, K. (2009). A parallel circuit of LIF signalling pathways maintains pluripotency of mouse ES cells. *Nature* **460** 118–122.
- ROBINSON, J. W. and HARTEMINK, A. J. (2009). Nonstationary dynamic Bayesian networks. *Adv. Neural Inf. Process. Syst.* **21** 1369–1376.
- ROUDER, J. N., SPECKMAN, P. L., SUN, D., MOREY, R. D. and IVERSON, G. (2009). Bayesian t tests for accepting and rejecting the null hypothesis. *Psychon. Bull. Rev.* **16** 225–237.
- SADDEH, M. J., MOFFA, G. and SPANG, R. (2013). Considering unknown unknowns-reconstruction of nonconfoundable causal relations in biological networks. In *Research in Computational Molecular Biology* 234–248. Springer, Berlin.
- SMALL, J. V., GEIGER, B., KAVERINA, I. and BERSHADSKY, A. (2002). How do microtubules guide migrating cells? *Nat. Rev. Mol. Cell Biol.* **3** 957–964.
- SONG, L., KOLAR, M. and XING, E. P. (2009). Time-varying dynamic Bayesian networks. *Adv. Neural Inf. Process. Syst.* **22** 1732–1740.

- TRESCH, A. and MARKOWETZ, F. (2008). Structure learning in nested effects models. *Stat. Appl. Genet. Mol. Biol.* **7** Art. 9, 28. [MR2386326](#)
- VAN DEN BERG, D. L., ZHANG, W., YATES, A., ENGELEN, E., TAKACS, K., BEZSTAROSTI, K., DEMMERS, J., CHAMBERS, I. and POOT, R. A. (2008). Estrogen-related receptor beta interacts with Oct4 to positively regulate Nanog gene expression. *Mol. Cell. Biol.* **28** 5986–5995.
- VASKE, C. J., HOUSE, C., LUU, T., FRANK, B., YEANG, C.-H., LEE, N. H. and STUART, J. M. (2009). A factor graph nested effects model to identify networks from genetic perturbations. *PLoS Comput. Biol.* **5** e1000274, 16. [MR2486699](#)

CANCER RESEARCH UK CAMBRIDGE INSTITUTE
UNIVERSITY OF CAMBRIDGE
LI KA SHING CENTRE
ROBINSON WAY
CAMBRIDGE, CB2 0RE
UNITED KINGDOM
E-MAIL: xinwang2hms@gmail.com
ke.yuan@cruk.cam.ac.uk
florian.markowetz@cruk.cam.ac.uk
URL: <http://www.markowetzlab.org/>